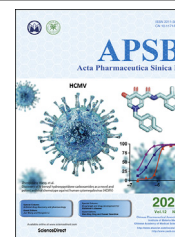




Chinese Pharmaceutical Association  
Institute of Materia Medica, Chinese Academy of Medical Sciences

Acta Pharmaceutica Sinica B

[www.elsevier.com/locate/apsb](http://www.elsevier.com/locate/apsb)  
[www.sciencedirect.com](http://www.sciencedirect.com)



ORIGINAL ARTICLE

# A practical strategy to develop isoform-selective near-infrared fluorescent probes for human cytochrome P450 enzymes



Lei Feng<sup>a,b,†</sup>, Xiangge Tian<sup>b,†</sup>, Dahong Yao<sup>c</sup>, Zhenlong Yu<sup>b</sup>,  
Xiaokui Huo<sup>a,b</sup>, Zhenhao Tian<sup>d</sup>, Jing Ning<sup>b,\*</sup>, Jingnan Cui<sup>d</sup>,  
Tony D. James<sup>e,f</sup>, Xiaochi Ma<sup>a,b,\*</sup>

<sup>a</sup>Second Affiliated Hospital, Dalian Medical University, Dalian 116023, China

<sup>b</sup>College of Pharmacy, the National & Local Joint Engineering Research Center for Drug Development of Neurodegenerative Disease, Dalian Medical University, Dalian 116044, China

<sup>c</sup>School of Pharmaceutical Sciences, Shenzhen Technology University, Shenzhen 518060, China

<sup>d</sup>State Key Laboratory of Fine Chemicals, Dalian University of Technology, Dalian 116024, China

<sup>e</sup>Department of Chemistry, University of Bath, Bath BA2 7AY, UK

<sup>f</sup>School of Chemistry and Chemical Engineering, Henan Normal University, Xinxiang 453007, China

Received 5 September 2021; received in revised form 20 October 2021; accepted 16 November 2021

## KEY WORDS

Enzyme activity  
bioimaging;  
Cytochrome P450;  
Drug–drug interactions;  
Biomarker analysis;  
Fluorescent probe

**Abstract** Currently, the development of selective fluorescent probes toward targeted enzymes is still a great challenge, due to the existence of numerous isoenzymes that share similar catalytic capacity. Herein, a double-filtering strategy was established to effectively develop isoenzyme-specific fluorescent probe(s) for cytochrome P450 (CYP) which are key enzymes involving in metabolism of endogenous substances and drugs. In the first-stage of our filtering approach, near-infrared (NIR) fluorophores with alkoxy group were prepared for the screening of CYP-activated fluorescent substrates using a CYPs-dependent incubation system. In the second stage of our filtering approach, these candidates were further screened using reverse protein-ligand docking to effectively determine CYP isoenzyme-specific probe(s). Using our double-filtering approach, probes **S9** and **S10** were successfully developed for the real-time and selective detection

**Abbreviations:** CYP, cytochrome P450; DDI, drug–drug interactions; DNZ, danazol; FVT, fluvastatin; HLM, human liver microsome; ICT, intra-molecular charge transfer; LC–MS/MS, liquid chromatography–tandem mass spectrometry; MCN, miconazole; MD, molecular dynamics; MM-GBSA, binding free energy calculation; NADPH, nicotinamide-adenine dinucleotide phosphate; NIR, near-infrared; PT, prothrombin time; RMSD, root-mean square deviation; RLX, raloxifene; SPN, sulfaphenazole; SCN, sulconazole; WAR, warfarin.

\*Corresponding authors. Tel.: +86 411 86110419.

E-mail addresses: [ningjing0626@163.com](mailto:ningjing0626@163.com) (Jing Ning), [maxc1978@163.com](mailto:maxc1978@163.com) (Xiaochi Ma).

†These authors made equal contributions to this work.

Peer review under responsibility of Chinese Pharmaceutical Association and Institute of Materia Medica, Chinese Academy of Medical Sciences

<https://doi.org/10.1016/j.apsb.2021.11.019>

2211-3835 © 2022 Chinese Pharmaceutical Association and Institute of Materia Medica, Chinese Academy of Medical Sciences. Production and hosting by Elsevier B.V. This is an open access article under the CC BY-NC-ND license (<http://creativecommons.org/licenses/by-nc-nd/4.0/>).

of CYP2C9 and CYP2J2, respectively, to facilitate high-throughput screening and assessment of CYP2C9-mediated clinical drug interaction risks and CYP2J2-associated disease diagnosis. These observations suggest that our strategy could be used to develop the isoform-specific probes for CYPs.

© 2022 Chinese Pharmaceutical Association and Institute of Materia Medica, Chinese Academy of Medical Sciences. Production and hosting by Elsevier B.V. This is an open access article under the CC BY-NC-ND license (<http://creativecommons.org/licenses/by-nc-nd/4.0/>).

## 1. Introduction

Cytochrome P450 (CYP) is a large group of HEME-containing monooxygenases that can catalyze the oxidative metabolism of endogenous and exogenous chemicals mainly through dealkylation, hydroxylation, and epoxidation reactions<sup>1</sup>. CYP1A2, 2B6, 2C8, 2C9, 2C19, 2D6, 2J2, 3A4/5 are well-known members of CYP1-4 subfamily, and they have attracted much attention due to their prominent roles in the metabolism of drug and exogenous toxicants, as the important phase I xenobiotic-metabolizing enzymes found in the human liver<sup>2–4</sup>. According to statistics, the xenobiotic-metabolizing CYP are participated in the metabolism of approximately 80% of drugs<sup>5,6</sup>. Thus, inhibition or induction of CYP enzymes is a frequent cause of clinical drug–drug interactions (DDI). Notably, the inhibition of CYP activity by co-administrated drugs may alter clinical outcomes or even lead to life-threatening adverse reactions, which are closely related to the safety of particular medication used in clinic<sup>7,8</sup>. For instance, CYP2C9 inhibition has been recognized as a major reason for the life-threatening clinical DDI of warfarin which is a widely used anticoagulant, where hemorrhaging is often caused by elevated plasma concentration<sup>9,10</sup>. Hence, it is a significant public health issue for evaluating CYPs activity and associated DDI risk, particularly the CYP metabolized drugs that exhibit a narrow therapeutic window (*e.g.*, CYP2C9 and warfarin)<sup>11</sup>. Additionally, a few subtypes of CYP family play significant roles in diverse physiological and pathological processes through regulation of the metabolism of endogenous biologically active substances<sup>12–14</sup>. Some CYP isoenzymes, such as CYP2J2, have been associated with tumorigenesis such as cell proliferation, apoptosis, and tumor metastasis<sup>15,16</sup>. Therefore, the highly sensitive and specific molecular tools for characterizing the real-time activity of CYP isoenzymes in complex biological systems, would be of particular benefit for disease treatment applications and evaluation of medicines in clinic.

Currently, the detection of CYPs activity relies mainly on high-performance liquid chromatography or hyphenated techniques with mass spectrometry<sup>17,18</sup>. Unfortunately, these approaches are unsuitable for the detection of live-specimens or *in vivo* applications, thus seriously limiting the ability for real-time tracking of enzymatic activity, and evaluating the functional variation of endogenous CYPs under various physiological and pathological conditions<sup>19</sup>. Fluorescent probes have been extensively used as useful molecular tools, that can facilitate the noninvasive imaging and dynamic monitoring of enzymatic activity in complex living systems<sup>20–27</sup>. Imaging probes that exhibit near-infrared (NIR) optical signals have many advantages including minimal interference from tissue autofluorescence and improved tissue penetration, which facilitates imaging allowing for accurate activity monitoring of functional proteins in living systems<sup>28–33</sup>. However,

to date the number of selective NIR fluorescent probes for real-time imaging of various CYP isoforms are limited.

In practice, there are many challenges remaining for the development of selective NIR fluorescent probe toward target CYP isoforms, since CYPs are a HEME protein superfamily composed of many homologous proteins sharing similar catalytic functions and substrate spectra<sup>34</sup>. The pronounced substrate overlap for numerous CYPs poses a major obstacle in the development of probes for specifically sensing a CYP subtype. For instance, 7-ethoxyresorufin, is a widely used fluorescent probe for the CYP1A subfamily<sup>35,36</sup>, and 7-benzyloxyquinoline is a commonly used tool to screen modulators of the CYP3A subfamily<sup>37</sup>. However, the low selectivity and short emission wavelength of these probes seriously hinders the accurate evaluation of target CYP activity in complex living organisms, which limit their practical applications. As such the main challenge in the development of CYP fluorescent probes is how to overcome problems associated with the interaction between various CYPs and small molecule fluorophores, to rapidly screen candidate(s) with preferred isoform-selectivity and metabolic reaction. Unfortunately, there remains a lack of practical strategies for the effective design and development of enzyme-activated fluorescent probes with high specificity toward target CYP isoenzymes.

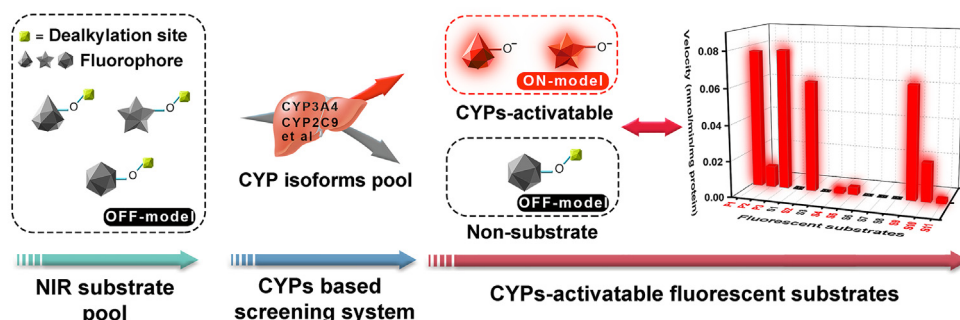
In our present work, a novel double-filtering strategy was developed to uncover CYP isoenzyme-specific NIR fluorescent probes, based on the catalytic and structure characteristics of human CYPs (Scheme 1). In the first-stage of screening, a series of NIR fluorophores introduced a methoxy group, were synthesized due to dealkylation as a preferential reaction of numerous CYP isoforms. These potential fluorescent substrates were then subjected to filtering using CYP-dependent *in vitro* screening system, and constructed a substrate pool of CYPs-activated NIR fluorescent probes. In the second-stage of filtering, the NIR fluorescent substrate candidates were screened using reverse protein–ligand docking between fluorescent substrates and human CYPs (Scheme 1B) in order to determine potential isoenzyme-specific CYPs probes. For each fluorescent substrate candidate, a CYP isoform-catalytic selectivity spectrum could be generated according to the calculated catalytic distance and relative binding energy. Using our double-filtering approach, two probes (**S9** and **S10**) were successfully established for the real-time and selective detection of CYP2C9 and CYP2J2, respectively. These observations suggest that our new strategy is useful to effectively develop the isoform-specific probes for CYPs.

## 2. Materials and methods

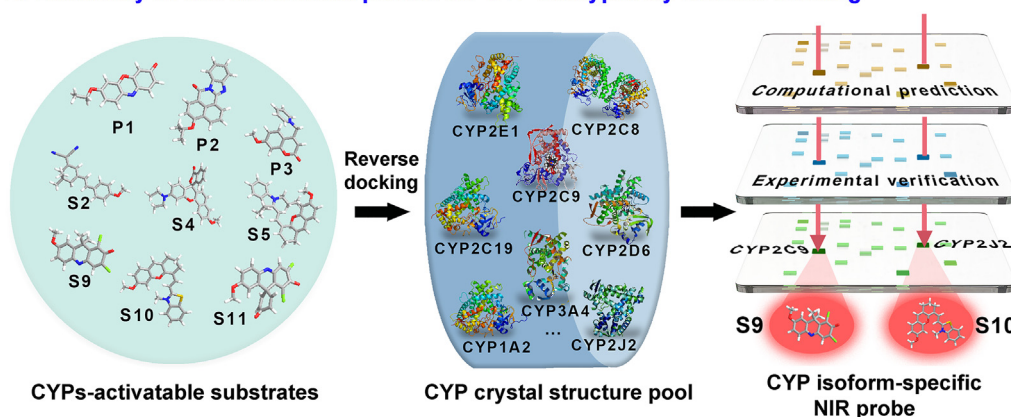
### 2.1. Materials and reagents

Recombinant human cytochrome P450 isoenzymes (rhCYP) were purchased from Cypex (Dundee, UK). The human liver microsomes (50-Donor, LOT: IHG) were obtained from Bioreclamation IVT

### A. Activity-based *in vitro* screening of NIR fluorescent substrates for CYPs



### B. Discovery of NIR fluorescent probes for CYP subtypes by reverse docking



**Scheme 1** Double-filtering strategy consists of CYPs activity-based screening and reverse protein–ligand docking to discover CYP isoenzyme-specific NIR fluorescent probes. (A) *In vitro* metabolic activity screening of alkylated NIR substrate pool through CYP isoforms pool. (B) Computational screening of the NIR fluorescent probe(s) by reverse protein–ligand docking to develop catalytic spectra (schematically displayed using a chip diagram labelled computational prediction). The experimental verification ‘chip’ represents the incubation results of recombinant CYP isoforms, were consistent with those using the double-filtering strategy (illustrated using the overlapped ‘chip’ bottom). **P1–P3** are known fluorescent probes for CYPs. Finally, the isoform-selective fluorescent probes (**S9** and **S10**) toward CYP isoforms (2C9 and 2J2) were determined.

(MD, USA). D-Glucose-6-phosphate (G-6-P, LOT: WXBC5003V), glucose-6-phosphate dehydrogenase (LOT: SLBJ9913V), NADP sodium salt (LOT: BCCD0008), sulfaphenazole (LOT: 083H0050) were obtained from Sigma–Aldrich (MO, USA). Raloxifene (LOT: J0206A), sulconazole (LOT: N1211AS), fluvastatin (LOT: J0701A), quinidine (LOT: M0110A), omeprazole (LOT: D0929As), clomethiazole (LOT: D1225A), 8-methoxypsoralen (LOT: M0113A), tetraethylenepentamine (TEPA, LOT: S0801A), ticlopidine (LOT: A0606AS) were purchased from Meilun Biotechnology (Dalian, China). Prothrombin time assay kit purchased from Nianjing Jiancheng Bioengineering Institute (Nanjing, China). The purity of DDAO and HXMB was >98%. All other reagents were of the highest grade commercially available.

#### 2.2. Docking-based virtual screening

Molecular docking: the initial enzyme structures and their corresponding PDB entry ID are listed as follows: CYP1A1 (4I8V), CYP1A2 (2HI4), CYP1B1 (3PM0), CYP2A6 (2FDW), CYP2A13 (4EJG), CYP2B6 (4I91), CYP2C8 (2NNI), CYP2C9 (1R90), CYP2C19 (4GQS), CYP2D6 (4WNU), CYP2E1 (3E6I), CYP3A4 (1W0E), CYP3A5 (5VEU). For the other applied CYP structures

as CYP2J2, 4A11, 4F2, 4F3B and 4F12, the homology modeling and molecular dynamic simulation run for 20 ns were used for their three-dimensional coordinate building and optimization. Subsequently, the protonation state of residues was carefully assigned and initially preserved water molecules in crystal structure were deleted. Parameters for proteins were described based on Charmm force field. The Discovery Studio 3.5 docking program was then adopted<sup>38</sup>. The Goldscore was selected as the score function, and the other parameters were set as default. From each docking study, a total of 10 docking poses were generated with corresponding root-mean square deviation (RMSD) values being calculated.

Molecular dynamics (MD) simulations: before the final production run, the modeled systems were firstly minimized by three rounds simulation procedures with successively relaxed restraints. The heating process from 0 to 310 K for each of the modeled system was ran for 50 ps. In order to equilibrate the system without any restraint, all the systems were again running for 500 ps. The production phase of the simulations was carried out for a total of 100 ns. The MD simulations were all performed using the Amber 10 package<sup>39</sup>. The particle mesh Ewald summation was used to handle the long-range coulombic interactions. The

SHAKE algorithm was employed for all atoms covalently bonded with a hydrogen atom. The time step of 2 fs was set for sampling in production run.

Binding free energy calculation (MM-GBSA): the binding free energy calculation was performed using the MM-GBSA scripts embedded in AMBER10. Snapshots were extracted every 10 ps from the MD trajectory.

### 2.3. Enzyme kinetic analysis

Briefly, rhCYP2C9 (7.5 pmol/mL) or rhCYP2J2 (5 pmol/mL) was incubated with DDAM or MXMB in incubation mixture (200  $\mu$ L), which consisted of NADPH-generating system and potassium phosphate buffer (100 mmol/L, pH 7.4). Incubation substrate or inhibitor was dissolved in DMSO and the final concentration of DMSO was controlled below 1% (v/v) in the mixtures. After 30 or 10 min incubation at 37  $^{\circ}$ C, add acetonitrile to terminate the reaction, and centrifuge the sample at 20,000 $\times$ g. The fluorescence metabolite was detected. Kinetic parameters were analyzed using GraphPad Prism 7.0 (GraphPad Software, Inc., CA, USA).

### 2.4. CYP2C9 modulators high-throughput screening

The modulation effect of clinical drugs and herbal medicines toward CYP2C9 were assayed in 96-well microplates with fluorescent image analyzer ( $\lambda_{\text{ex}}$  of 635 nm,  $\lambda_{\text{em}}$  of 670  $\pm$  15 nm). A mixture of DDAM (10  $\mu$ mol/L), clinical drugs (10  $\mu$ mol/L) or extracts of traditional Chinese medicine (20  $\mu$ g/mL) and HLM was incubated at 37  $^{\circ}$ C in potassium phosphate buffer in the present of NADPH-generating system.

The inhibitory effects of CYP2C9 inhibitors (miconazole, MCN; sulconazole, SCN; fluvastatin, FVT; raloxifene, RLX; sulfaphenazole, SPN) toward CYP2C9 were evaluated by incubating with DDAM and modulators with series of concentrations (0.1, 0.5, 1, 10 and 20  $\mu$ mol/L). The % residual activities of all samples were calculated. Then the data were fitted to a log (inhibitor) vs. normalized response in GraphPad Prism 7.0 (GraphPad Software, Inc., CA, USA).

### 2.5. Pharmacokinetic and pharmacodynamic drug interactions with CYP2C9 inhibitor

The experiments were performed in accordance with guidelines approved by the ethics committee of Dalian Medical University (AEE19047). The inhibitory effects of MCN on the metabolism of warfarin were investigated in rats. The rats (SD rat, male) randomly grouped to two test group. The rats in MCN group were treated with MCN (oral, 30 mg/kg) 30 min before being given an oral dose of warfarin (0.2 mg/kg). The rats in control group were treated with vehicle control instead of MCN. The plasma concentration of warfarin in rats from the different treatment groups were detected by LC/MS/MS that performed with an AB SCIEX QTRAP 5500. The liquid chromatographic sample analyses instrument was a Waters UPLC system equipped with 2998 Photodiode Array detector. The liquid separation was performed by Luna Omega Polar C<sub>18</sub> column (2.1 mm  $\times$  100 mm, 3  $\mu$ m). Acetonitrile/water (0.1% formic acid) in a starting volume ratio of 6.5:3.5 to 1.5 min, and then transitions to 9:1 in 1 min, with the flow rate was 0.4 mL/min. The quantitation of warfarin was accomplished by MRM with the transitions  $m/z$  306.7/205.2. The system was operated in the negative mode at  $-4500$  V. The

operating conditions were set as follows: CE,  $-30$  V; ion source temperature, 600  $^{\circ}$ C; DP,  $-120$  V; CXP,  $-5$  V; EP,  $-10$  V.

Male C57BL/6 mice were used to investigate the effect of MCN on the pharmacodynamics of warfarin. The mice were treated with MCN for four consecutive oral doses with 2 h interval. The mice were given a single oral dose of warfarin (1 mg/kg) 30 min after the last administration of MCN (50 mg/kg). The pharmacodynamic interactions were evaluated by monitoring and comparing the prothrombin time (PT) of the mice from different treatment groups.

### 2.6. Cell culture and imaging

HeLa and HepG2 cells were cultured in RPMI-1640 and DMEM containing 10% FBS, respectively. Cells were seeded in 6-well plates (100,000 cells/well). After overnight incubation, the plate was washed with FBS-free medium, and the probe MXMB (10  $\mu$ mol/L) was added. The albumin nanoparticles of DDAM were prepared by desolvation process, which were used to cell imaging. Then, the cells were incubated for 1 h at 37  $^{\circ}$ C, and washed with PBS. The cells were then imaged with a confocal microscope (Leica SP8, Germany). Images were acquired with excitation at 633 nm and a fluorescence emission window of 650–690 nm for DDAM, and 690–750 nm for MXMB.

### 2.7. Angiogenesis assays

HUVEC (DMEM containing 0.1% BSA) were seeded on matrigel coated Ibitreat angiogenesis slides (20,000 cells/slide) and evaluated the tube formation, as previous described<sup>40,41</sup>. Tubular structure was imaged with a confocal microscope (Leica SP8, Germany). Endothelial cell spheroids were generated as previous described<sup>42</sup>. After 6, 24 and 48 h in a collagen gel, and angiogenesis was imaged with a confocal microscope (Leica SP8, Germany). Images were acquired as described above.

### 2.8. In vivo imaging of CYP2J2 in tumor-bearing mice

The experiments were performed in accordance with guidelines approved by the ethics committee of Dalian Medical University (AEE19047). HeLa and HepG2 cells (5,000,000 cells in PBS) were injected subcutaneously into nude mice, respectively. When the tumors grown to a suitable size for imaging, MXMB (50  $\mu$ mol/L) was injected into the solid tumors. Imaging was performed at 0–60 min by virtue of an *in vivo* imaging system (PerkinElmer IVIS, USA). The multi-spectral imaging was obtained from 670 to 730 nm and excited at 630 nm.

## 3. Results and discussion

### 3.1. Construct double-filtering strategy to develop selectivity fluorescent probes

The pronounced substrate overlap for numerous CYPs poses a major obstacle in the development of highly selective probes for sensing a given CYP subtype. As such the main challenge for the development of CYP fluorescent probes is how to overcome the key problems associated with the interaction between various CYPs and small molecule fluorophores, to rapidly screen candidate(s) with preferred isoform-selectivity and metabolic reaction. With this research, a novel double-filtering strategy was developed to uncover CYP isoenzyme-specific NIR fluorescent probes, based

on the CYP isoforms pool-based activity screening and virtual screening using reverse protein-ligand docking (Scheme 1).

In the first-stage of screening, a series of NIR fluorescent substrates were designed comprehensive consideration of fluorescence mechanism and the metabolic preference of CYP enzymes (S1 to S11, Supporting Information Fig. S1). These probes with a potential CYP-mediated fluorescence OFF to ON model, were then subjected to filtering by using CYP-dependent human liver microsome (HLM, CYP isoforms pool) system with NADPH. The *in vitro* preliminary screening was used to effectively construct a substrate pool of CYPs-activated NIR fluorescent probes, including S2, S4, S5, S9, S10 and S11 (Fig. 1A).

In the second-stage of filtering, the NIR fluorescent substrate candidates were screened using reverse protein-ligand docking between methylated fluorophores and the three-dimensional (3D) structures of human CYPs (Scheme 1B) in order to determine potential isoenzyme-specific CYPs probes. Using the 3D structures of CYPs include CYP1A1, 1A2, 1B1, 2A6, 2A13, 2B6, 2C8, 2C9, 2C19, 2D6, 2E1, 2J2, 3A4, 3A5, 4A11, 4F2, 4F3B and 4F12, the distances from Fe atom of the CYP HEME to the dealkylation site of these fluorescent candidates were evaluated. When the catalytic distance exceeded an appropriate range for CYP mediated catalysis (3–6 Å), the fluorescent substrates were less likely to be dealkylated. For each fluorescent candidate, a CYP isoform-catalytic spectrum could be generated according to the calculated catalytic distance. These fluorescent substrates were then subjected to molecular dynamics simulations and free energy calculations using the generalized Born surface area continuum solvation (MM/GBSA) methods.

The relative catalytic efficiency spectrum of the CYPs (Fig. 1B) was constructed using the relative values of binding energy for different CYP subtypes, which represented the selectivity of each fluorescent candidate toward various CYP isoforms. In order to confirm the reliability of this method, three known fluorescent probes for CYPs (P1, P2, P3, Supporting Information Fig. S1) were introduced as control molecules into the fluorescent probe candidate pool, and the selectivity predicted by the CYP

catalytic spectrum, correlated well with the isoform-selectivity previously reported<sup>3,35,36,43,44</sup>. Additionally, the predicted results obtained using the fluorescent substrates agreed with the experimental results of the *in vitro* incubation assays using recombinant human CYP isoforms (Supporting Information Fig. S2), which confirmed the reliability and advantages of our double-filtering approach for the rapid development of CYP fluorescent probes with high isoform-selectivity. Finally, as shown in Fig. 1B, S9 and S10 were discovered as the potential isoform selective and NIR fluorescent probes of CYP2C9 and CYP2J2, respectively. The underlying interaction mechanism of DDAM (S9, Fig. 1C) or MXMB (S10, Fig. 1D) with their corresponding metabolic enzymes (CYP2C9 or CYP2J2) were then elucidated using molecular dynamic simulations and docking.

### 3.2. Spectral properties of DDAM and MXMB

The spectral response of DDAM toward CYP2C9 was first explored. It was observed a fluorescence spectrum with an emission maximum at 658 nm upon excitation at 600 nm (Fig. 2A). Upon the addition of different concentrations of CYP2C9 to the incubation mixtures with DDAM, the fluorescence intensity at 658 nm increased linearly (Fig. 2B;  $R^2 = 0.9941$ ,  $y = 2437x - 1984$ ). Subsequent spectral response of MXMB toward CYP2J2 found that a marked fluorescence signal was formed which holding an emission maximum at 724 nm when excited at 670 nm (Fig. 2C). Furthermore, the fluorescence intensity at 724 nm increased linearly when the concentration of CYP2J2 was varied from 1.0 to 12.5 pmol/mL (Fig. 2D;  $R^2 = 0.9993$ ,  $y = 57.49x - 16.51$ ). These fluorescence responses confirmed the intramolecular charge transfer (ICT) induced by CYP2C9-mediated dealkylation of DDAM and CYP2J2-mediated dealkylation of MXMB (Fig. 3A and C). DDAO showed strong fluorescence with maxima at 658 nm over pH range of 5–11 in contrast to the extremely weak fluorescence of DDAM (Supporting Information Fig. S3). Similarly, a discernible change in the fluorescence emission of HXMB was observed in comparison with MXMB over pH range of

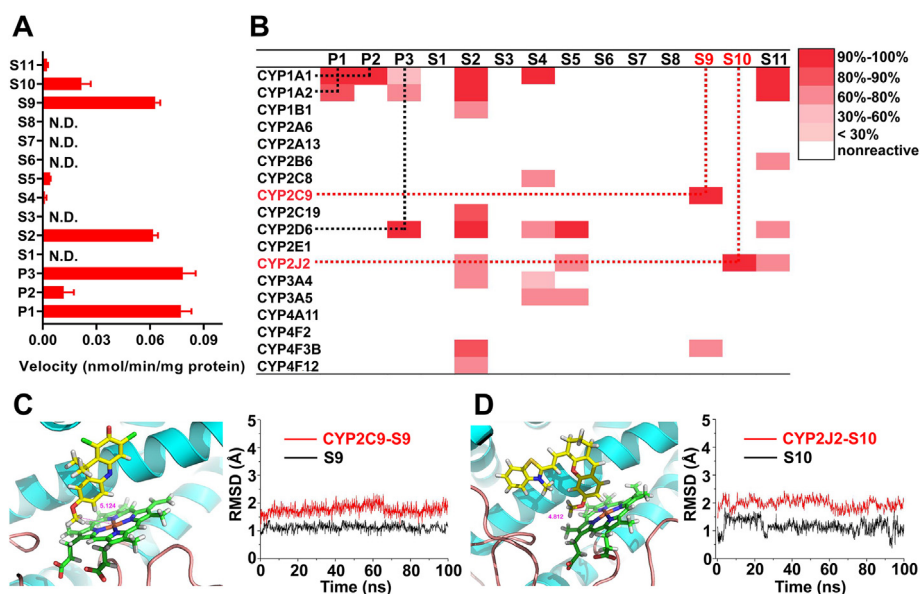


**Figure 1** (A) Dealkylation rates of NIR fluorescent substrates by CYP-dependent human liver microsome (HLM). (B) Reverse protein-ligand docking predicted selectivity catalytic spectrum of CYPs for the designed NIR fluorescent substrates. P1, P2 and P3 are known fluorescent probes of CYPs. S1–S11 are the designed fluorescent substrates of CYPs. (C) Docking simulation (left) and molecular dynamic simulations (right) of S9 into CYP2C9. (D) Docking simulation (left) and molecular dynamic simulations (right) of S10 into CYP2J2.

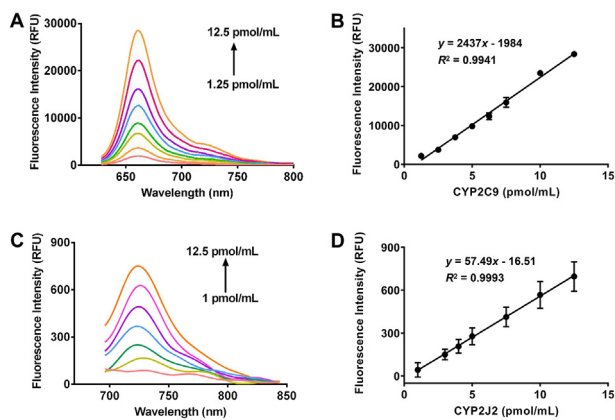


**Figure 2** Fluorescence response of DDAM (S9) and MXMB (S10) toward CYP2C9 and CYP2J2. Fluorescence spectra (A) and fluorescence intensity (B) of DDAM with increasing concentrations of CYP2C9 (1.25–12.5 pmol/mL),  $\lambda_{ex}/\lambda_{em} = 600/658$  nm. Fluorescence spectra (C) and fluorescence intensity (D) of MXMB with increasing concentrations of CYP2J2 (1.0–12.5 pmol/mL),  $\lambda_{ex}/\lambda_{em} = 670/724$  nm.

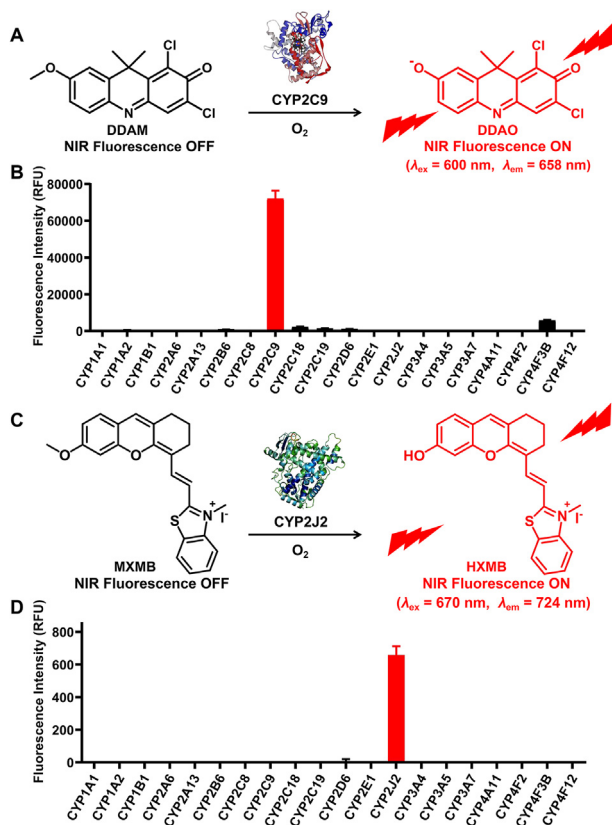


**Figure 3** Proposed mechanism of CYP2C9 (A) and CYP2J2 (C) triggering the fluorescence response of DDAM and MXMB. Fluorescence response of DDAM (B) and MXMB (D) following incubation with various human CYP isoenzymes, respectively.

7–11 (Supporting Information Fig. S4). These results demonstrated that DDAM and MXMB could be used to determine the activity of CYP2C9 and CYP2J2 under physiological conditions (pH 7.4), respectively.

### 3.3. Selectivity and metabolic properties of DDAM and MXMB

The selectivity of DDAM (S9) and MXMB (S10) for CYP isoenzymes was then evaluated using a series of *in vitro* incubation experiments. As shown in Fig. 3B, CYP2C9 produced remarkable fluorescence enhancement at 658 nm, over other CYP isoenzymes. Moreover, the various potential interfering species hardly influenced the fluorescence response of DDAM, which exhibited high selectivity for CYP2C9 (Supporting Information Fig. S5). Inhibition assays were performed using some specific inhibitors for CYP isoenzymes to confirm the specificity of DDAM. The demethylation of DDAM was inhibited by sulfaphenazole as a selective inhibitor of CYP2C9 (Supporting Information Fig. S6), confirming the high selectivity of DDAM toward CYP2C9. Similarly, CYP2J2 produced remarkable fluorescence enhancement at 724 nm over other CYP isoenzymes when MXMB was incubated with individual forms of recombinant human CYP (Fig. 3D). Meanwhile, a series of similar experiments were performed to confirm the specificity of MXMB to human CYP2J2 (Supporting Information Figs. S7 and S8).

Subsequently, the metabolic properties of DDAM and MXMB were investigated, respectively. CYP2C9 mediated demethylation of DDAM exhibited Michaelis–Menten kinetics (Supporting Information Fig. S9), where the apparent substrate affinity constant ( $K_m$ ) and maximum rate constant ( $V_{max}$ ) of CYP2C9 for DDAM-*O*-demethylation were determined to be 3.8  $\mu\text{mol/L}$  and 1.31 nmol/min/nmol P450 (Supporting Information Table S1). Additionally, CYP2J2 mediated MXMB-*O*-demethylation exhibited good reactivity, and  $K_m$  and  $V_{max}$  were determined to be 0.51  $\mu\text{mol/L}$  and 22.89 nmol/min/nmol P450, respectively (Supporting Information Fig. S9 and Table S1). These characteristics of DDAM and MXMB indicated high sensitivity for sensing CYP2C9 and CYP2J2, respectively. Accordingly, the excellent selectivity and sensitivity of DDAM and MXMB as well as their near-infrared fluorescence output should enable the precise and sensitive detection of the corresponding CYP isoenzyme in complex biological systems.

### 3.4. High-throughput screening of CYP2C9 modulators based on DDAM

CYP2C9 is abundantly expressed in the human liver, and can metabolize approximately 20% of clinical drugs, some of which are narrow therapeutic index drugs<sup>45,46</sup>. As such molecular tools that could be used to selectively detect the CYP2C9 activity and further rapidly assess the DDI risks of CYP2C9, would be of great benefit for the rational usage in clinical medicine. In previous studies, the risk assessment of CYP2C9-mediated DDI was determined (1) using LC–MS/MS method for detecting metabolites formed in incubation system of human liver microsomes; (2) or based on recombinant human CYP2C9 combining with mass spectrometry or fluorescence methods<sup>47</sup>. The former assay is susceptible to the interference from other CYP2C enzymes due to the insufficient selectivity of probe substrate, while the real physiological environment of CYP2C9 was ignored in the later assay, which limited the *in vitro-in vivo* extrapolation of DDI risk of CYP2C9. Therefore, there is an urgent need for a highly selective fluorescent substrate to facilitate the real-time detection of CYP2C9 in complex biological systems.

In the present study, we employed DDAM-*O*-demethylation as the probe reaction to rapidly screen CYP2C9 modulators from 93

commonly used clinical drugs visually *via* fluorescence imaging using human liver microsome incubation system. The high-throughput and visual assays in a 96-well-microplate were used to successfully screen five strong inhibitors (A7: raloxifene, RLX; B4: sulconazole, SCN; C5: miconazole, MCN; G1: fluvastatin, FVT; G5: sulfaphenazole, SPN) and eight activators (A6: omeprazole; A8: dapsone; B7: mebendazole; B10: pantoprazole; D3: loratadine; E10: estradiol; F6: dopamine; F8: lansoprazole) toward CYP2C9 (Fig. 4A, H10, H11 and H12 are control samples). The series of modulators such as MCN, SCN, FVT, RLX and SPN mentioned above, exhibited significant inhibitory effect toward CYP2C9 in a concentration-dependent manner (Fig. 4B). Moreover, the inhibitory effects of clinical drugs toward CYP2C9 measured using our high-throughput fluorescence assay agreed with the corresponding results obtained using the microplate reader (Supporting Information Fig. S11), which indicated the accuracy and practicability of our fluorescence strategy. To further verify the application of CYP2C9 modulator screening for resolving practical clinical problems of DDI, the risk of warfarin induced bleeding was assessed during co-administration of the strong inhibitor (MCN) for CYP2C9 *in vivo*. From a pharmacokinetic (PK) view, co-administration of MCN can significantly increase the plasma exposure to warfarin in experimental animals where the maximum blood concentration ( $C_{max}$ ) and area under the curve (AUC) were 169% and 85% higher, respectively, when compared with the control group that were solely administrated

warfarin (Fig. 4D, Supporting Information Table S2). Furthermore, the dramatic change in the exposure level to warfarin lead to pharmacodynamic variations in the experimental animals. The prothrombin times (PT) of animals administrated with a combination of MCN and warfarin were significantly prolonged (Fig. 4E), and life-threatening subcutaneous abdominal wall hemorrhaging was observed.

Additionally, the highly efficient and sensitive screening method could be used to effectively uncover some novel natural modulators of CYP2C9 from complex sample containing diversified chemical components. As such, the inhibitory effects of herbal medicines and the involved specific inhibitory components were investigated with the aid of DDAM high-throughput and visual fluorescence assay (Fig. 5). Several extracts of herbal medicines exhibited strong inhibitory effects toward CYP2C9, including *Agrimonia pilosa* Ledeb. (A3), *Evodia rutaecarpa* (Juss.) Benth. (A9) and *Eupatorium japonicum* Thunb. (A10). Furthermore, 1-methyl-2-undecyl-4(1H) quinolone was successfully identified as the novel inhibitor of CYP2C9 from *E. rutaecarpa* (Juss.) Benth. (Fig. 5C). Additionally, DDAM could also be used for real-time imaging the endogenous CYP2C9 in living cells (Supporting Information Fig. S12). Therefore, DDAM, as a visible molecular tool for detecting CYP2C9 activity, could be used to construct a high-throughput screening system for the assessment of clinical DDI risk mediated by human CYP2C9 in complex biospecimens.

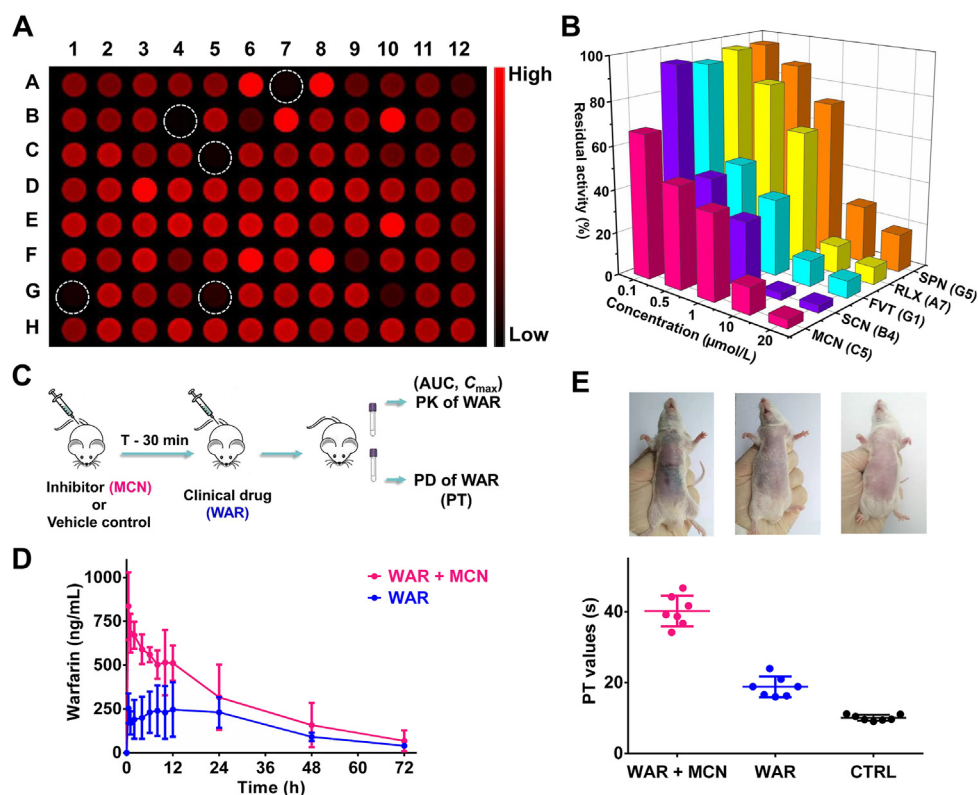


**Figure 4** Inhibitory effects of various clinical drugs toward human CYP2C9. (A) Visual fluorescence response to the regulatory effects of clinical drugs on CYP2C9 activity after incubation with DDAM in 96-well microplates measured by the fluorescent image analyzer ( $\lambda_{ex}$ : 635 nm,  $\lambda_{em}$ :  $670 \pm 15$  nm, H10, H11 and H12 are control samples). (B) Concentration-dependent inhibitory effects of 5 inhibitors against CYP2C9. (C) Schematic illustration of the administration of CYP2C9 inhibitor MCN and clinical drug warfarin (WAR). Effects of MCN treatment on the pharmacokinetics (D) and pharmacodynamics (E) of WAR. PT, prothrombin time. Picture of the subcutaneous abdominal wall haemorrhage for experimental animals from different treatment groups.

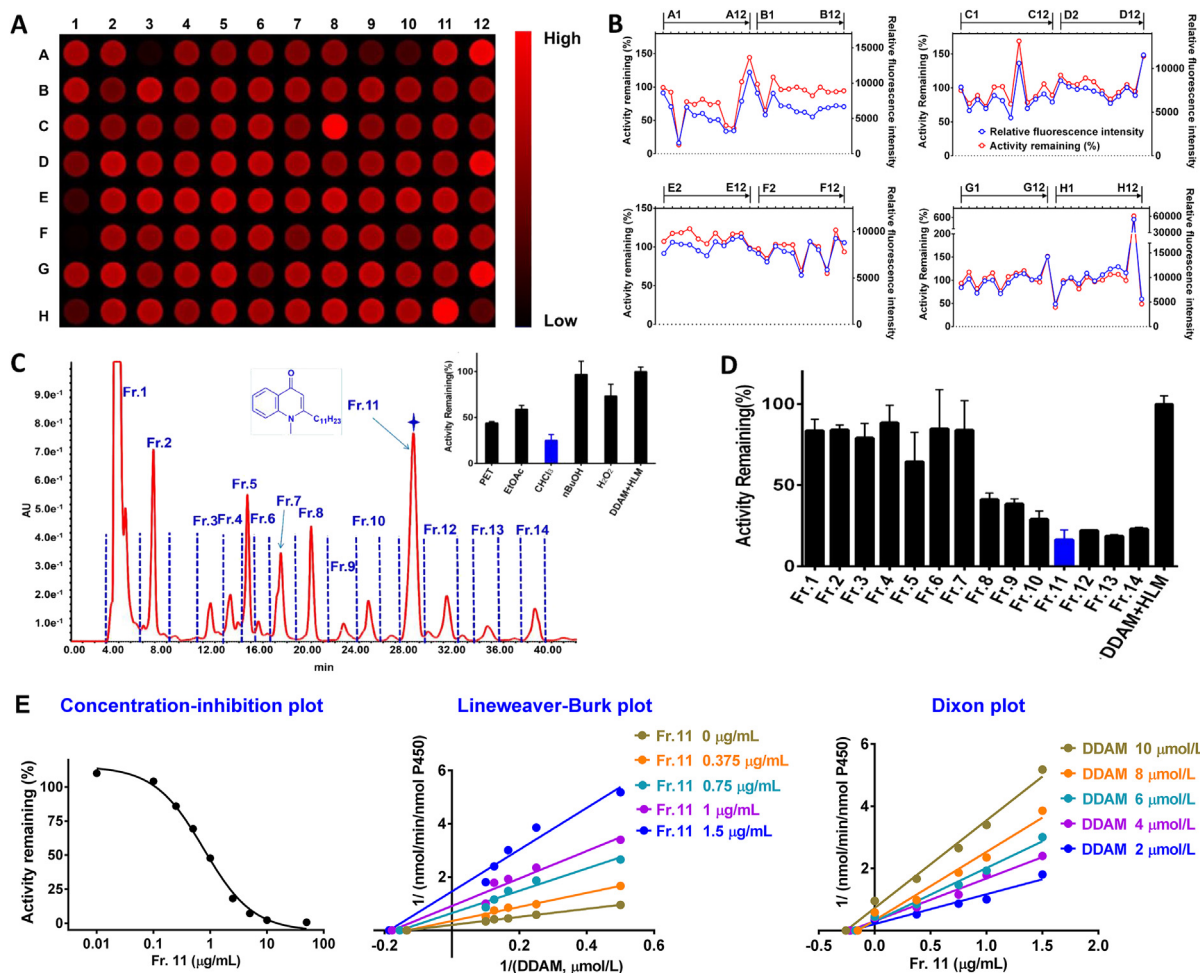


**Figure 5** Inhibitory effects of herbal medicines toward human CYP2C9. (A) Fluorescence image response to the inhibitory action of extracts of herbal medicines against CYP2C9 after incubation with DDAM in 96-well microplates measured by fluorescent image analyzer ( $\lambda_{\text{ex}}$ : 635 nm,  $\lambda_{\text{em}}$ : 670  $\pm$  15 nm, A1, B1 and C1 are control samples, D1, E1 and F1 are positive control samples treated with 0.1, 1, 10  $\mu\text{mol/L}$  miconazole, respectively). (B) Corresponding inhibitory effects of herbal medicines on CYP2C9 were measured using the present fluorescence assay (red) by the fluorescent image analyzer ( $\lambda_{\text{ex}}$ : 635 nm,  $\lambda_{\text{em}}$ : 670 nm  $\pm$  15 nm) and relative fluorescence intensity (blue) based on microplate reader ( $\lambda_{\text{ex}}$ : 600 nm,  $\lambda_{\text{em}}$ : 658 nm), respectively. (C) HPLC chromatogram of chloroform extracts of *Evodia rutaecarpa* (Juss.) Benth. and prepared fraction profiles. The activity remaining of CYP2C9 in presence of individual extracts was inserted. (D) Inhibitory effects of the pre-HPLC fractions from the extracts of *Evodia rutaecarpa* (Juss.) Benth. toward CYP2C9. (E) The  $\text{IC}_{50}$  and inhibition kinetics of CYP2C9 by fraction 11 (Fr. 11) of *Evodia rutaecarpa* (Juss.) Benth.

### 3.5. Bioimaging of angiogenesis and tumors based on MXMB

CYP2J2 was a novel potential biomarker for cancer diagnosis and treatment, owing to its key role in proliferation, apoptosis, and angiogenesis of primary tumors<sup>15,16</sup>. Thus, real-time sensing and imaging of CYP2J2 activity in tumor is highly desirable in clinic. In the present study, HeLa and HepG2 were used as model cell lines to demonstrate the potential of the fluorescent probe (MXMB) for the determination of endogenous CYP2J2 activity in living biospecimen. After the cells were incubated with MXMB, it was observed a drastic enhancement of the fluorescence signal in HeLa and HepG2 cells (Fig. 6A). Pre-treatment with CYP2J2 inhibitor danazol (DNZ) resulted in a remarkable suppression of intracellular fluorescence due to reduced formation of HXMB mediated by CYP2J2 (Supporting Information Fig. S13). Furthermore, MXMB can be used to clearly image tubular

morphogenesis of human umbilical vein endothelial cells (HUVEC) in an *in vitro* angiogenesis model (Fig. 6B). Assisted by 3D imaging, the spatial structure of the tubes composed of HUVEC could be clearly observed at a penetration depth of about 200  $\mu\text{m}$ . The monitoring ability of MXMB for neovessel formation was verified using real-time imaging of CYP2J2 with the 3D angiogenesis models (Fig. 6B). Furthermore, the time-dependent dynamic processes of neovessels sprouting from 3D spheroids could be visualized, facilitating the real-time tracking of angiogenesis in malignant neoplasms.

Subsequently, the applicability of MXMB for the *in vivo* imaging of CYP2J2 activity in tumors was evaluated. A fluorescence signal was rapidly observed in the tumor region after *in vivo* injection of MXMB. The average fluorescence intensity in HeLa and HepG2 cell-transplanted tumor at 60 min post-injection was determined, and was proportional to the expression level of

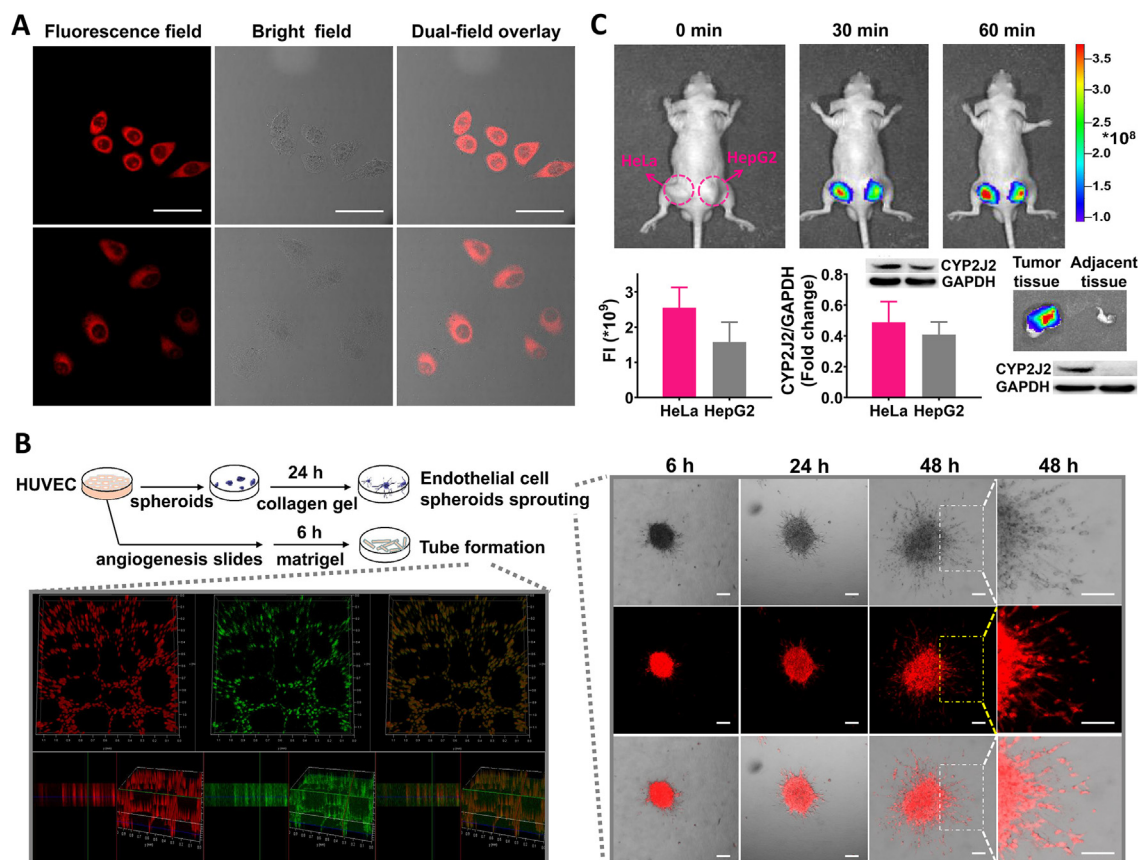


**Figure 6** Fluorescence bioimaging of CYP2J2 *in vitro* and *in vivo*. (A) Confocal fluorescence imaging of CYP2J2 activities by MXMB in HeLa (Top) and HepG2 (Bottom) cells. Scale bar is 50  $\mu\text{m}$ . (B) Confocal fluorescence imaging of tube formation and endothelial cell spheroids sprouting by MXMB in angiogenesis assays. Insert: schematic of the angiogenesis experiment. 2D and 3D confocal fluorescence imaging of tube formation. Time-dependent dynamic imaging of neovessels sprouting from 3D spheroids at 6, 24 and 48 h. MXMB (red,  $\lambda_{\text{ex}}$ : 633 nm,  $\lambda_{\text{em}}$ : 690–750 nm), FITC-Lectin (green,  $\lambda_{\text{ex}}$ : 543 nm,  $\lambda_{\text{em}}$ : 590–650 nm), scale bar is 100  $\mu\text{m}$ . (C) *In vivo* imaging in tumor-bearing nude mice after tumor injection. Activities and protein levels of CYP2J2 in tumor *in vitro* and *in vivo* were performed, respectively. FI, fluorescence intensity ( $\text{p/s/cm}^2/\text{sr}$ )/( $\mu\text{W/cm}^2$ ).

CYP2J2 in the corresponding tumor samples (Fig. 6C). Additionally, the strong fluorescence signal observed in HepG2 cell-transplanted tumor when compared with that of adjacent tissue indicated the high specificity for tumor tracing of MXMB, and the specificity was further verified by comparison with CYP2J2 protein content in tumor tissues. Taken together, it has been comprehensively evaluated the utility of MXMB for the real-time detection of CYP2J2 *in vitro* and *in vivo*, which facilitated the visualization of CYP2J2-associated cancer cells, angiogenesis and neoplasm.

#### 4. Conclusions

In summary, using a novel double-filtering strategy which provides a new practical approach to develop CYP isoenzyme-selective fluorescent substrates, we have developed two NIR fluorescent probes for the selective and sensitive detection of CYP isoenzymes. DDAM has been used for sensing CYP2C9 activity and high-throughput screening of CYP2C9 modulators, which could provide useful guidance in the assessment of clinical DDI risks mediated by CYP2C9. While, MXMB could be selectively activated by CYP2J2 in various tumor models, thereby facilitating

the real-time and multi-dimensional tracking of CYP2J2 activity in various living biological systems. More importantly, the present strategy is more broad-spectrum and practical, and the combination of ‘real’ screening and ‘virtual’ screening of our strategy may provide new idea for developing other enzyme-activated and isoform-specific fluorescent probes.

#### Acknowledgments

The authors thank the National Natural Science Foundation of China (81930112, 82174228 and 82004211), National Key R&D program of China (2018YFC1705900), Distinguished Professor of Liaoning Province (XLYC2002008, China), “1+X” program for Clinical Competency enhancement-Interdisciplinary Innovation Project of Second Hospital of Dalian Medical University, Dalian Science and Technology Leading Talents Project (2019RD15, China), High-level Talents of Dalian (2020RQ066 and 2020RQ076, China), the Open Research Fund of the School of Chemistry and Chemical Engineering, and Henan Normal University for support (2020ZD01 and 2021YB07, China) for financial support. T.D.J. wishes to thank the Royal Society for a Wolfson Research Merit Award.

### Author contributions

Xiaochi Ma and Jing Ning conceptualized and conceived the project and edited the manuscript. Lei Feng and Xiangge Tian contributed equally, performed the experiments, analyzed the data, and wrote the original manuscript. Dahong Yao, Zhenlong Yu, Xiaokui Huo, and Zhenhao Tian performed partial experiments. Jingnan Cui and Tony D. James involved in data analysis and provided valuable advice. All authors discussed the results and participated in analyzing the experimental results.

### Conflicts of interest

The authors declare no conflicts of interest.

### Appendix A. Supporting information

Supporting information to this article can be found online at <https://doi.org/10.1016/j.apsb.2021.11.019>.

### References

- Bernhardt R. Cytochromes P450 as versatile biocatalysts. *J Biotechnol* 2006;**124**:128–45.
- Redlich G, Zanger UM, Riedmaier S, Bache N, Giessing ABN, Eisenacher M, et al. Distinction between human cytochrome P450 (CYP) isoforms and identification of new phosphorylation sites by mass spectrometry. *J Proteome Res* 2008;**7**:4678–88.
- Feng L, Ning J, Tian XG, Wang C, Yu ZL, Huo XK, et al. Fluorescent probes for the detection and imaging of cytochrome P450. *Coord Chem Rev* 2021;**437**:213740.
- Wu JJ, Guan XQ, Dai ZR, He RJ, Ding XX, Yang L, et al. Molecular probes for human cytochrome P450 enzymes: recent progress and future perspectives. *Coord Chem Rev* 2021;**427**:213600.
- Nebert DW, Russell DW. Clinical importance of the cytochromes P450. *Lancet* 2002;**360**:1155–62.
- Singh D, Kashyap A, Pandey RV, Saini KS. Novel advances in cytochrome P450 research. *Drug Discov Today* 2011;**16**:793–9.
- Wei P, Zhang J, Egan-Hafley M, Liang S, Moore DD. The nuclear receptor CAR mediates specific xenobiotic induction of drug metabolism. *Nature* 2000;**407**:920–3.
- Williams D, Feely J. Pharmacokinetic-pharmacodynamic drug interactions with HMG-CoA reductase inhibitors. *Clin Pharmacokinet* 2002;**41**:343–70.
- Rosenborg S, Stenberg M, Otto S, Ostervall J, Masquelier M, Yue QY, et al. Clinically significant CYP2C inhibition by nescapine but not by glucosamine. *Clin Pharmacol Ther* 2010;**88**:343–6.
- Ohlsson S, Holm L, Myrberg O, Sundström A, Yue QY. Nescapine may increase the effect of warfarin. *Br J Clin Pharmacol* 2008;**65**:277–8.
- Vazquez SR. Drug–drug interactions in an era of multiple anticoagulants: a focus on clinically relevant drug interactions. *Blood* 2018;**132**:2230–9.
- Murray GI. The role of cytochrome P450 in tumour development and progression and its potential in therapy. *J Pathol* 2000;**192**:419–26.
- McDougle DR, Watson JE, Abdeen AA, Adili R, Caputo MP, Krapf JE, et al. Anti-inflammatory  $\omega$ -3 endocannabinoid epoxides. *Proc Natl Acad Sci U S A* 2017;**114**:E6034–43.
- Yeboah MM, Hye Khan MA, Chesnik MA, Skibba M, Kolb LL, Imig JD. Role of the cytochrome P-450/epoxyeicosatrienoic acids pathway in the pathogenesis of renal dysfunction in cirrhosis. *Nephrol Dial Transplant* 2018;**33**:1333–43.
- Jiang JG, Chen CL, Card JW, Yang S, Chen JX, Fu XN, et al. Cytochrome P450 2J2 promotes the neoplastic phenotype of carcinoma cells and is upregulated in human tumors. *Cancer Res* 2005;**65**:4707–15.
- Jiang JG, Ning YG, Chen C, Ma D, Liu ZJ, Yang S, et al. Cytochrome p450 epoxygenase promotes human cancer metastasis. *Cancer Res* 2007;**67**:6665–74.
- Kim MJ, Kim H, Cha IJ, Park JS, Shon JH, Liu KH, et al. High-throughput screening of inhibitory potential of nine cytochrome P450 enzymes *in vitro* using liquid chromatography/tandem mass spectrometry. *Rapid Commun Mass Spectrom* 2005;**19**:2651–8.
- Youdim KA, Saunders KC. A review of LC–MS techniques and high-throughput approaches used to investigate drug metabolism by cytochrome P450s. *J Chromatogr B Analyt Technol Biomed Life Sci* 2010;**878**:1326–36.
- Ning J, Wang W, Ge G, Chu P, Long F, Yang Y, et al. Targeted enzyme activated two-photon fluorescent probes: a case study of CYP3A4 using a two-dimensional design strategy. *Angew Chem Int Ed* 2019;**58**:9959–63.
- Wu X, Shi W, Li X, Ma H. A strategy for specific fluorescence imaging of monoamine oxidase A in living cells. *Angew Chem Int Ed* 2017;**56**:15319–23.
- Dai ZR, Feng L, Jin Q, Cheng HL, Li Y, Ning J, et al. A practical strategy to design and develop an isoform-specific fluorescent probe for a target enzyme: CYP1A1 as a case study. *Chem Sci* 2017;**8**:2795–803.
- Tian ZH, Ding LL, Li K, Song YQ, Dou TY, Hou J, et al. Rational design of a long-wavelength fluorescent probe for highly selective sensing of carboxylesterase 1 in living systems. *Anal Chem* 2019;**91**:5638–45.
- Jin Q, Ma HY, Feng L, Wang P, He RJ, Ning J, et al. Sensing cytochrome P450 1A1 activity by a resorufin-based isoform-specific fluorescent probe. *Chin Chem Lett* 2020;**31**:2945–9.
- Tian Z, Yan F, Tian X, Feng L, Cui J, Deng S, et al. A NIR fluorescent probe for Vanin-1 and its applications in imaging, kidney injury diagnosis, and the development of inhibitor. *Acta Pharm Sin B* 2022;**12**:316–25.
- Feng L, Tian Z, Zhang M, He X, Tian XG, Yu ZL, et al. Real-time identification of gut microbiota with aminopeptidase N using an activable NIR fluorescent probe. *Chin Chem Lett* 2021;**32**:3053–6.
- Zhang H, Fan J, Wang J, Zhang S, Dou B, Peng X. An off-on COX-2-specific fluorescent probe: targeting the Golgi apparatus of cancer cells. *J Am Chem Soc* 2013;**135**:11663–9.
- Chen S, Dong G, Wu S, Liu N, Zhang W, Sheng C. Novel fluorescent probes of 10-hydroxyevodiamine: autophagy and apoptosis-inducing anticancer mechanisms. *Acta Pharm Sin B* 2019;**9**:144–56.
- Wu X, Li L, Shi W, Gong X, Ma H. Near-infrared fluorescent probe with new recognition moiety for specific detection of tyrosinase activity: design, synthesis, and application in living cells and zebrafish. *Angew Chem Int Ed* 2016;**55**:14728–32.
- Guo Z, Park S, Yoon J, Shin I. Recent progress in the development of near-infrared fluorescent probes for bioimaging applications. *Chem Soc Rev* 2014;**43**:16–29.
- Ning J, Liu T, Dong P, Wang W, Ge G, Wang B, et al. Molecular design strategy to construct the near-infrared fluorescent probe for selectively sensing human cytochrome P450 2J2. *J Am Chem Soc* 2019;**141**:1126–34.
- Tong H, Lou K, Wang W. Near-infrared fluorescent probes for imaging of amyloid plaques in Alzheimer's disease. *Acta Pharm Sin B* 2015;**5**:25–33.
- Tian X, Liu T, Ma Y, Gao J, Feng L, Cui J, et al. Molecular-splicing strategy to construct a near-infrared fluorescent probe for UDP-glucuronosyltransferase 1A1. *Angew Chem Int Ed* 2021;**60**:24566–72.
- Huang J, Li J, Lyu Y, Miao Q, Pu K. Molecular optical imaging probes for early diagnosis of drug-induced acute kidney injury. *Nat Mater* 2019;**18**:1133–43.
- Gay SC, Roberts AG, Halpert JR. Structural features of cytochromes P450 and ligands that affect drug metabolism as revealed

- by X-ray crystallography and NMR. *Future Med Chem* 2010;**2**:1451–68.
35. Burke MD, Thompson S, Weaver RJ, Wolf CR, Mayer RT. Cytochrome P450 specificities of alkoxyresorufin *O*-dealkylation in human and rat liver. *Biochem Pharmacol* 1994;**48**:923–36.
  36. Schiwiy A, Brinkmann M, Thiem I, Guder G, Winkens K, Eichbaum K, et al. Determination of the CYP1A-inducing potential of single substances, mixtures and extracts of samples in the micro-EROD assay with H4IIE cells. *Nat Protoc* 2015;**10**:1728–41.
  37. Stresser DM, Turner SD, Blanchard AP, Miller VP, Crespi CL. Cytochrome P450 fluorometric substrates: identification of isoform-selective probes for rat CYP2D2 and human CYP3A4. *Drug Metab Dispos* 2002;**30**:845–52.
  38. Wu G, Robertson DH, Brooks 3rd CL, Vieth M. Detailed analysis of grid-based molecular docking: a case study of CDOCKER-A CHARMM-based MD docking algorithm. *J Comput Chem* 2003;**24**:1549–62.
  39. Case DA, Cheatham TE, Darden T, Gohlke H, Luo R, Merz KM, et al. The Amber biomolecular simulation programs. *J Comput Chem* 2005;**26**:1668–88.
  40. Shi L, Fisslthaler B, Zippel N, Frömel T, Hu J, Elgheznawy A, et al. MicroRNA-223 antagonizes angiogenesis by targeting  $\beta$ 1 integrin and preventing growth factor signaling in endothelial cells. *Circ Res* 2013;**113**:1320–30.
  41. Kiefer FN, Munk VC, Humar R, Dieterle T, Landmann L, Battegay EJ. A versatile *in vitro* assay for investigating angiogenesis of the heart. *Exp Cell Res* 2004;**300**:272–82.
  42. Korff T, Augustin HG. Tensional forces in fibrillar extracellular matrices control directional capillary sprouting. *J Cell Sci* 1999;**112**:3249–58.
  43. Ning J, Tian ZH, Wang B, Ge GB, An Y, Hou J, et al. A highly sensitive and selective two-photon fluorescent probe for real-time sensing of cytochrome P450 1A1 in living systems. *Mater Chem Front* 2018;**2**:2013–20.
  44. Venhorst J, Onderwater RC, Meerman JH, Commandeur JN, Vermeulen NP. Influence of *N*-substitution of 7-methoxy-4-(aminomethyl)-coumarin on cytochrome P450 metabolism and selectivity. *Drug Metab Dispos* 2000;**28**:1524–32.
  45. Miners JO, Birkett DJ. Cytochrome P450 2C9: an enzyme of major importance in human drug metabolism. *Br J Clin Pharmacol* 1998;**45**:525–38.
  46. Williams PA, Cosme J, Ward A, Angove HC, Vinković DM, Jhoti H. Crystal structure of human cytochrome P450 2C9 with bound warfarin. *Nature* 2003;**424**:464–8.
  47. Zhou SF, Zhou ZW, Yang LP, Cai JP. Substrates, inducers, inhibitors and structure–activity relationships of human cytochrome P450 2C9 and implications in drug development. *Curr Med Chem* 2009;**16**:3480–675.